JOURNAL OF GEOPHYSICAL RESEARCH, VOL. 100, NO. A11, PAGES 21,375–21,383, NOVEMBER 1, 1995

Altitude profiles of localized *D* region density disturbances produced in lightning-induced electron precipitation events

Sean J. Lev-Tov, Umran S. Inan, and Timothy F. Bell

STAR Laboratory, Department of Electrical Engineering, Stanford University, Stanford, California

Abstract. A three-dimensional model of very low frequency (VLF) radio wave propagation in the Earth-ionosphere waveguide in the presence of lower ionospheric disturbances is used to quantitatively interpret VLF signatures of lightning-induced electron precipitation (LEP) events observed in two previously reported cases. One case is that of a 28.5-kHz signal originating in Puerto Rico and propagating to a receiver in Lake Mistissini, Quebec. The other case involves a 24.0-kHz signal originating in Cutler, Maine, and received at Stanford, California. In both cases, high-resolution measurements of the VLF signals were made to accurately document characteristic signatures of LEP events (Inan et al., 1988b, 1990). The comparison of the model calculations with the data yields information about the altitude profiles of electron density of both the extra ionization produced by the LEP events and of the ambient ionospheric *D* region. The comparisons are carried out using generally accepted values of the spatial extent of the disturbed regions and the intensity of the particle flux constituting the LEP burst.

Introduction

During the past few years the effects of lightning-induced electron precipitation (LEP) on VLF signals propagating in the Earth-ionosphere waveguide have been regularly observed as characteristically rapid (less than 1 s) changes in signal amplitude and phase, followed by a slower (10 to 100 s) recovery period [*Inan and Carpenter*, 1987]. The events have been temporally and, in some cases, geographically linked to lightning strikes through data on both spherics and whistler waves [*Lohrey and Kaiser*, 1979; *Carpenter and LaBelle*, 1982; *Inan and Carpenter*, 1986; *Inan et al.*, 1988a, b], both of which are produced by the lightning. Whistler waves traveling though the Earth's magnetosphere interact with geomagnetically trapped energetic electrons, changing their pitch angles. The result is that the mirroring heights of some electrons are lowered, and some precipitate into the lower ionosphere, causing secondary ionization in the *D* region which alters the amplitude and phase of VLF signals propagating though the Earth-ionosphere waveguide [*Helliwell et al.*, 1973]. LEP events represent a loss of particles from the Earth's radiation belts; quantitative interpretation of VLF signatures of these events may allow an assessment of the global significance of this loss of radiation belt electrons [*Burgess and Inan*, 1993].

Our goal is to model LEP events and the resulting VLF signal perturbations. By comparing our modeling results to data, we hope to assess the likely precipitated particle energy spectrum. A three-dimensional and multiple mode Earth-ionosphere waveguide VLF propagation model [*Poulsen et al.*, 1993] was employed to simulate the effects of LEP events on the perturbed VLF signals. The model was applied to the propagation paths of the perturbed VLF signals for three different ambient ionospheric electron density profiles, several different LEP event enhanced electron density profiles, events of different spatial size, and different disturbance locations (with respect to the paths). Ranges of the predicted amplitude changes of the VLF signal at the onset of events were compared to the data presented in two previously published cases. In one case [*Inan et al.*, 1988b], causative lightning activity associated with LEP events observed on a VLF propagation path was measured to be within ±150 km of the path. In the second case [*Inan et al.*, 1990], LEP events were observed simultaneously on two different crossing VLF propagation paths, indicative of the likely location of the ionospheric disturbances (assuming that the LEP was contained to a single duct).

Paper number 95JA01615.
0148-0227/95/95JA-01615$05.00

Review of Experimental Data

Case 1: NAU-LM, March 13,1987

Inan et al. [1988b] reported the observations during 0000 to 1200 UT on March 13, 1987 of perturbations on the subionospheric 28.5-kHz VLF signal propagating along the great circle path from the NAU transmitter in Puerto Rico to Lake Mistissini (LM), Quebec (Figure 1 and Table 1). Two types of perturbations were identified which occurred during different periods: early/fast events and LEP events. Classification of the events into the two categories was done by noting the time delay between the causative spheric and the onset of its event. In this study we are concerned with the perturbations identified as LEP events (Figure 2). The source of the causative lightning data was cloud-to-ground (CG) lightning flashes recorded by the SUNY-Albany east-coast lightning-detection network and radio atmospherics data from narrow-band VLF channels (tuned to other VLF signals received at LM).

On the NAU-LM signal, all of the LEP events were observed as signal level decreases; no phase data were available. The magnitude of the amplitude decreases ranged from the detection threshold of −0.1 dB to a maximum of −1.5 dB. The stronger CG flashes and those closer to the path were found to be the more likely to be accompanied by VLF perturbations. Most of the lightning activity was located within ±150 km (transverse distance) of the path.

Case 2: NAA-SU and 485-SA, October 10, 1987

In the work by *Inan et al.* [1990], VLF signal data acquired at night during October 1987 from a network of paths were considered. The data were screened for characteristic LEP event signatures. The

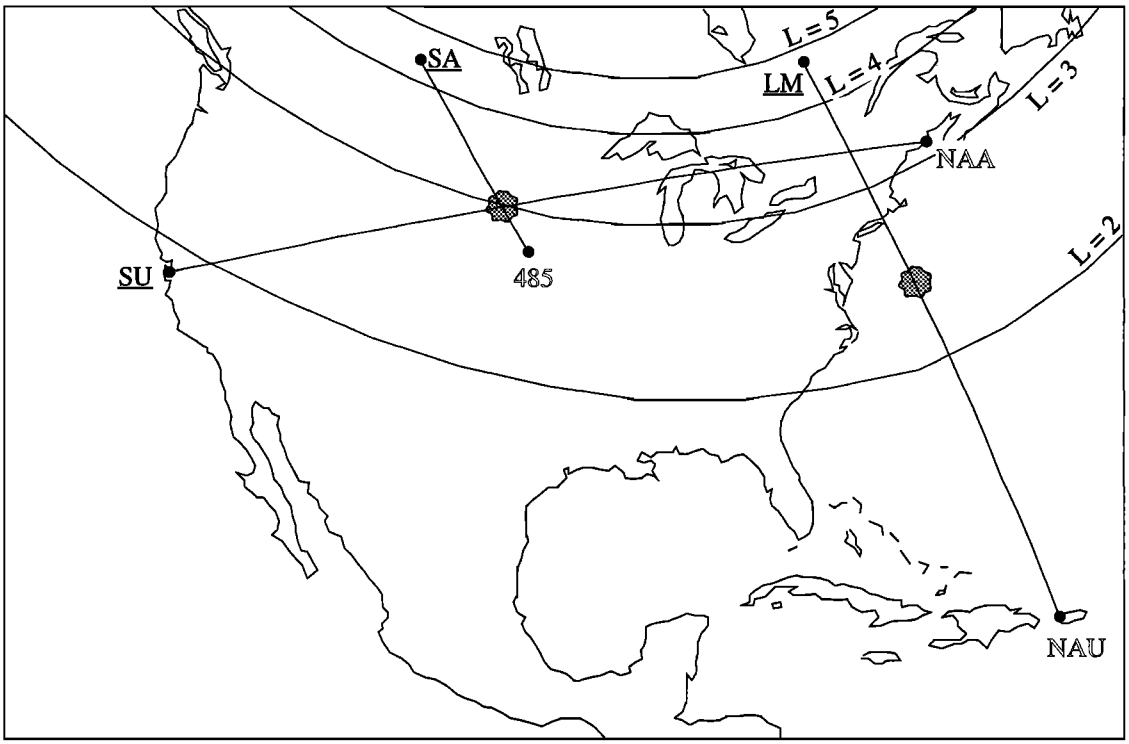

Figure 1. Map showing the VLF propagation paths between transmitters NAA, 48.5, and NAU and receivers SU, SA, and LM. Shaded regions indicate likely locations of ionospheric disturbances produced by lightning-induced electron precipitation (LEP).

case analyzed here involved activity on the path from the 24.0 kHz NAA transmitter in Maine to Stanford University (SU). The largest perturbation seen was about −0.5 dB (smaller perturbations were between −0.1 and −0.5 dB). Simultaneous perturbation events were observed on the path from the 48.5-kHz transmitter in Nebraska (referred to here as 485) to Saskatoon (SA), Saskatchewan. As Figure 1 shows, the two paths cross at nearly a right angle. Table 1 gives the coordinates of these transmitters and receivers. The fact that both 485-SA and NAA-SU were simultaneously perturbed is taken as evidence of the disturbance location being near the vicinity of the crossing point (44°N, 100°W) of the two paths [*Inan et al.*, 1990]; we make this assertion with the reservation that we are assuming that there is only one duct excited.

Computer Modeling

The present study makes use of a computer model of VLF radio wave propagation in the Earth-ionosphere waveguide in the presence of localized *D* region disturbances. This model is described in detail by *Poulsen et al.* [1993]. The model is based on a three-dimensional multimode calculation of VLF signal propagation through a realistic (in terms of both the ground and ionospheric conductivities, as well as the Earth's magnetic field) Earth-ionosphere waveguide. Various parameters can be adjusted in the model, including the spatial extent, location, and electron density profile of the disturbance, and the ambient ionospheric electron density profile and ground conductivity.

For each case considered, the model was applied with the three different ambient electron density profiles (1, 2, 3) shown in Figure 3a. Profile 1 is an exponential [*Wait and Spies*, 1964] which represents a tenuous nighttime ionosphere. Profile 2 displays typical conditions for the nighttime ionosphere [*Reagan et al.*, 1981]. Profile 3 represents a dense nighttime ionosphere [*Inan et al.*, 1992].

Table 1. VLF Transmitters and Receivers

Label	Frequency, kHz	Latitude	Longitude
NAA	24.0	45°N	67°W
NAU	28.5	18°N	67°W
485	48.5	42°N	98°W
LM	receiver	50°N	74°W
SA	receiver	51°N	107°W
SU	receiver	37°N	122°W

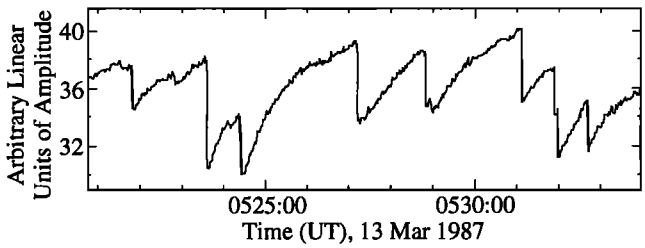

Figure 2. VLF signatures of LEP events observed on the NAU signal at LM. Each event exhibits the characteristic rapid amplitude change followed by a slower recovery period. The episode of events observed on this day were extensively documented in the work by *Inan et al.* [1988b].

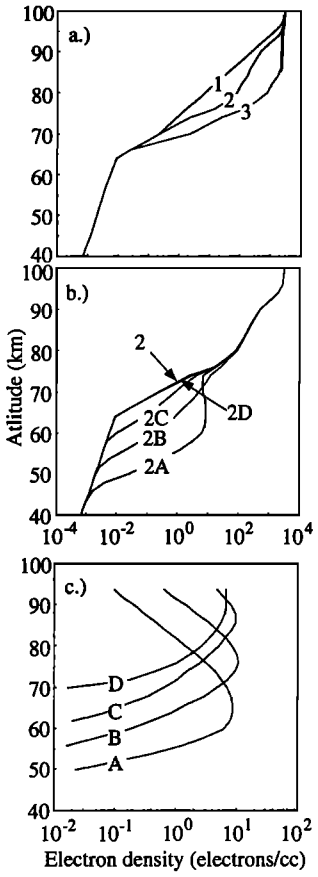

Figure 3. Nighttime electron density profiles used in this work. (a) Three ambient nighttime electron density profiles varying from a tenuous (1) to a dense (3) *D* region in a 1:10:100 range in the middle of the 70-90 km portion of the ionosphere where VLF reflection occurs at night. (b) The electron density profiles which were assumed to be in effect at the center of the disturbed regions. For the case illustrated, the ambient profile 2 is shown with the four ionization enhancements of the lower panel. (c) The excess ionization produced by different LEP bursts consisting of precipitating electrons with different energy spectra. It is this excess ionization which is added to the ambient electron density profiles (Figure 3a) to obtain the profile at the center of the LEP disturbance (Figure 3b).

The top portion of each profile is taken from the International Reference Ionosphere [*Rawer et al.*, 1978] and represents the region lying above 97 km for profile 1, above 90 km for profile 2, and above 95 km for profile 3. The three profiles encompass a 1:10:100 range of electron density values in the middle of the important altitude range of 70-90 km, near the nighttime VLF reflection height. For simplicity and because the ambient *D* region electron density is generally not known, the ambient electron density profile was taken to be the same everywhere along and near the great circle path. In addition, the ambient magnetic field magnitude and direction and ground conductivity were taken to be uniform everywhere, the values being chosen to be the actual values at the center of the location of the disturbance. Although the assumption of an essentially homogeneous ambient waveguide with respect to the (horizontal) direction of signal propagation may not appear realistic, homogeneous and inhomogeneous waveguide cases which we ran gave results with no significant differences. The results with the inhomogeneous waveguides were done using actual values of ground conductivity and ambient magnetic field that occur and vary along the great circle VLF propagation paths.

The electron density profiles of secondary ionization enhancement produced in the *D* region by four different typical LEP bursts are displayed in Figure 3c. These enhancement profiles are added to one of the ambient profiles of Figure 3a to produce the total enhanced electron density profiles which are the LEP disturbances in the ionosphere. Using as an example (ambient) profile 2, Figure 3b shows four enhanced electron density profiles which correspond to the enhancements of Figure 3c.

The secondary ionization enhancement profiles (A, B, C, D) of Figure 3c can be expected for 0.2-s LEP burst durations and a peak flux of 5×10^{-3} ergs cm^2 s^{-1} when whistler-particle interactions occur near the geomagnetic equator at *L* shells of 1.5 to 3 and ducted magnetospheric whistlers range in frequency from 0.5 to 6 kHz [*Chang and Inan*, 1985]. The energy spectra of the precipitation corresponding to profiles shown were calculated as discussed by *Inan et al.* [1988a] using linear pitch angle scattering, a fixed-length interaction region, and equilibrium conditions for the energy and *L* dependence of the trapped particle flux [*Lyons and Thorne*, 1973]. The equatorial electron density as a function of *L* was assumed to be [*Park et al.*, 1978; *Brace and Theis*, 1974]

$$N_{eq}(L) = 10^{(-1.58L+6.31)} + 10^{(-0.36L+3.87)}$$

The precipitation energy spectra corresponding to A, B, C and D are shown in Figure 4 along with the corresponding *L* shells. Such a variation in spectra can also occur at a fixed *L* shell due to variations in whistler frequency ranges excited by different lightning flashes. Penetration of the precipitating electrons into the ionosphere and the production of secondary ionization was then modeled as decribed by *Pasko and Inan* [1994] to arrive at the profiles of Figure 3c.

The profiles shown in Figure 3b represent the electron density at the center of the disturbance, from where the density enhancement is assumed to fall off as a Gaussian function of radial distance. With N_e being the electron density at any given altitude, and r being the radial distance from the disturbance center, we have

$$N_e(r) = N_e(r = 0)e^{-(\frac{r}{r_0})^2}$$

where the disturbance radial scale (r_0) was initially chosen to be 75 km, consistent with past experimental evidence indicating 100-200 km as the diameter of the disturbances in the cases analyzed [*Inan et al.*, 1988b, 1990].

VLF signal amplitude (and phase) changes observed in association with LEP bursts are functions of several factors. First is

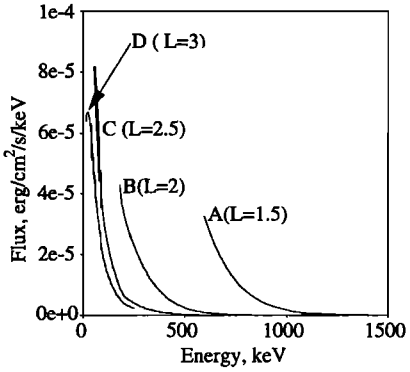

Figure 4. Differential flux of precipitated particles (in units of ergs cm^{-2} s^{-1} keV^{-1}) versus energy for different *L* shells of whistler-particle interaction.

the whistler (and therefore the lightning) intensity, which generally varies from event to event. Second are both the trapped and precipitated flux levels (the trapped flux level determines the precipitated flux level), which can also vary from event to event [*Inan et al.*, 1989]. Third is the spatial extent of the disturbance, which is determined predominantly by the size of the whistler-mode propagation duct and which therefore is most likely to remain constant during an episode of events. Fourth is the energy spectra of the precipitated particles which determines the altitude profile of electron density of the disturbance; the particle energy spectrum depends on the whistler frequency spectrum, the plasma frequency, the electron gyrofrequency, and the energy spectra of the gyroresonant particles with pitch angles near the loss cone [*Inan et al.*, 1989]. Fifth is disturbance location with respect to distance from the great circle path. The final factor is the ambient ionospheric electron density, which sets the VLF reflection height, thereby governing the mode structure of the VLF waveguide signal as it encounters the disturbance. In our present work, we explore the role of four of these contributing factors, the ambient and disturbed (secondary ionization enhancement) electron density profiles, the transverse position of the disturbance with respect to the great circle path, and the horizontal size of the disturbance.

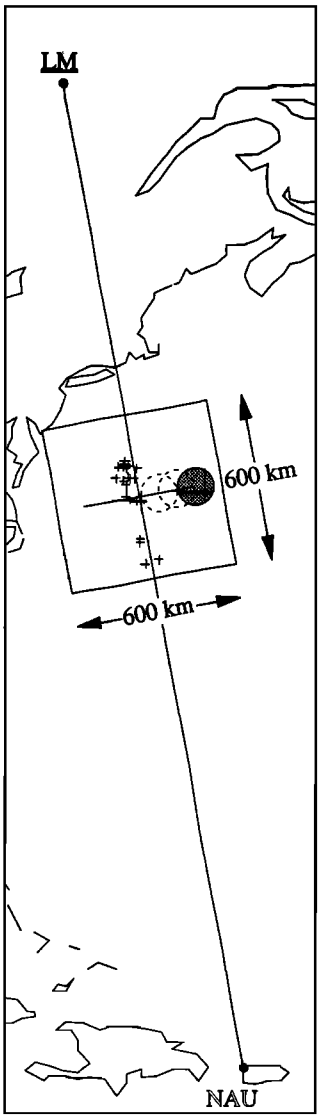

Figure 5. Expanded view of the NAU-LM path with the locations of cloud-to-ground lightning strikes recorded on March 13, 1987, during the hour of 0500-0600 UT. The circles represent sample locations of the disturbed region (150 km diameter, shown to scale) as it was moved along the scan line (thick line perpendicular to the VLF path) to produce data presented in Figures 6 and 9. The 600 × 600 km square defines the region wherein the disturbance was placed to generate Figure 7.

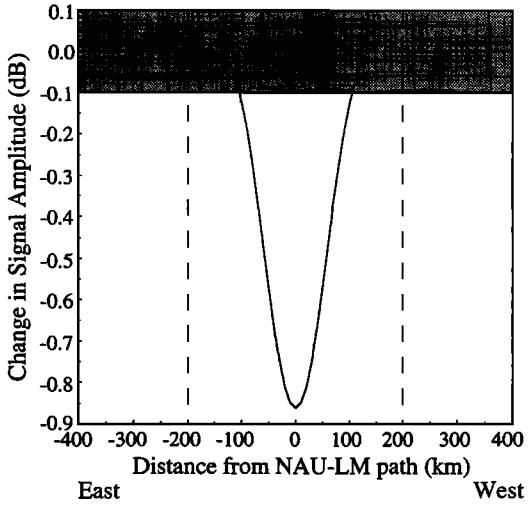

Figure 6. The predicted VLF amplitude change on the NAU signal at LM, with a 150-km-diameter disturbance while profile combination 2A is in effect. The abscissa corresponds to the scan line of Figure 5 but is extended up to 400 km on either side of the NAU-LM path. The shaded region shows the regime where signal amplitude changes are too small to be detectable.

Results

Case 1: NAU-LM, March 13, 1987

As a first step, model calculations were carried out for the 12 possible ambient (1, 2, 3) and disturbed (A, B, C, D) electron density profile combinations by varying for each case the position of the *D* region disturbance in a direction perpendicular to the NAU-LM path, as shown in Figure 5. Also shown for reference in Figure 5 is a sample of lightning discharges (shown by cross hairs) recorded by the lightning detection network during the period 0500-0600 UT. The scan line was chosen to be in the vicinity of lightning activity and is at a distance of 2100 km from NAU and 1520 km from the receiver (Lake Mistissini). Circles of diameter 150 km are shown along the scan line to indicate the size of the disturbance which was used in our modeling. Profile combination 2A resulted in the largest amplitude changes on the NAU signal (see below). Figure 6 is a plot of the change in signal amplitude versus position along the scan line for a 150-km-diameter disturbance for profile 2A. The shaded region bounded by ±0.1 dB represents the range within which the signal amplitude level changes are not detectable. As expected for the case of a homogeneous Earth-ionosphere waveguide, the amplitude changes as a function of disturbance position is symmetric about the great circle path. For the path in hand, and mainly because of the fact that the disturbance location is near the midpoint of a relatively long path, the amplitude change at the receiver does not depend sensitively on the location of the disturbance along the propagation

path. Adjacent scans 10 km apart were made within a region 600 × 600 km square shown in Figure 5, resulting in a surface plot of the expected change in signal amplitude as a function of the location of the disturbance, which is shown in Figure 7. For this case, profile combination 2A was used with a disturbance of diameter 150 km. It is apparent from Figure 7 that there is no discernible difference in signal level changes as a function of disturbance location parallel to the path within the square region shown.

In comparing model results with data by varying the ionospheric density profile, we have kept other parameters such as the size of the disturbance constant. Disturbances with greater transverse extent are generally expected to scatter a larger signal towards the receiver, thus leading to larger VLF perturbations [*Poulsen et al.*, 1993]. Figure 8 shows the change in signal level for profile combination 2A as a function of the diameter of the disturbance, which is centered on the great circle path.

We also note that the profiles of A, B, C, and D were obtained for a fixed value of peak precipitation flux equal to 5×10^{-3} ergs cm^2 s^{-1}. For LEP bursts with higher (lower) flux levels but having the same energy spectrum, the disturbance profiles would retain their shape (i.e., altitude variation) but simply increase (decrease) proportionally at all altitudes. Within the range of typical LEP burst flux levels of up to 10^{-2} ergs cm^2 s^{-1}, the scattering of the VLF signal would then be proportionally higher (lower) [*Poulsen et al.*, 1993], leading in most cases to larger (smaller) VLF amplitude changes. In the absence of direct information of the LEP burst flux levels, we have chosen to carry out our analysis for a moderate peak flux level of 5×10^{-3} ergs cm^2 s^{-1} [*Voss et al.*, 1984; *Inan et al.*, 1989].

Detailed comparison of the VLF amplitude changes as a function of disturbance location transverse to the path for a disturbance size of 150 km are shown in Figure 9 for the 12 different ionospheric profile combinations. It is clear that some profile combinations are not likely to lead to predicted NAU-LM perturbations consistent with observations. For example, noting that the observed VLF amplitude perturbations ranged from −0.1 to −1.5 dB [*Inan et al.*, 1988b], case 1A is ruled out since it would result in positive perturbations.

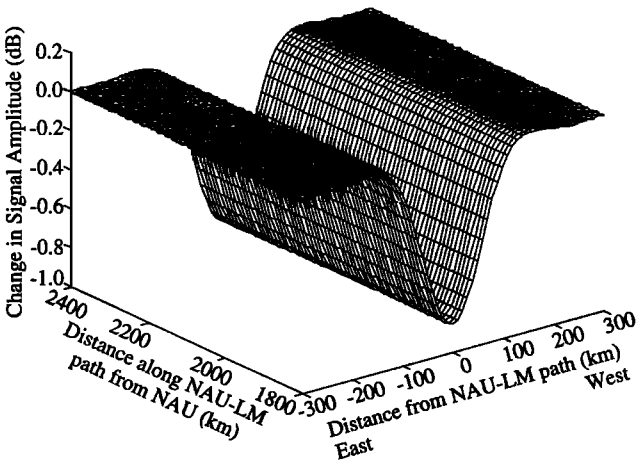

Figure 7. NAU signal amplitude change observed at LM as a function of the location of the ionospheric disturbance with respect to the great circle path. Profile combination 2A is used with a 150-km-diameter disturbance. The result shown covers the 600 × 600 km region shown in Figure 5. The fact that the VLF perturbation amplitudes are independent of disturbance location parallel to the path is evident.

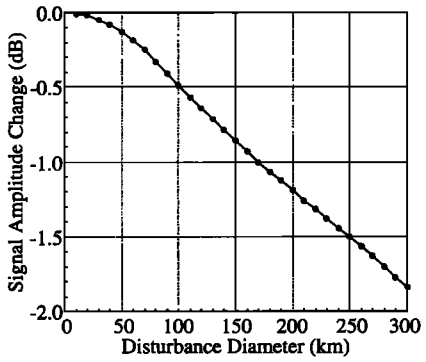

Figure 8. Amplitude change of the NAU signal at LM as a function of disturbance diameter. The disturbance is located on the great circle path at the center of the scan line shown in Figure 5, with profile combination 2A assumed to be in effect.

Under the assumptions of reasonable values of the peak precipitated flux (5×10^{-3} ergs cm^2 s^{-1}) and burst duration (0.2 s), we found that profile combination 2A results in signal amplitude changes (Figure 9) which are most consistent with the perturbations observed on the NAU signal received at LM. In addition, we find that although the bulk of the observed amplitude changes can be accounted for with a disturbance diameter of ~150 km, either a disturbance diameter of ~250 km (Figure 8) or higher precipitation flux levels is required to reproduce the full range of signal amplitude changes consistent with the data. It is thus possible that the largest of the observed events may have involved either higher fluxes or larger disturbance regions, or both.

Case 2: NAA-SU and 485-SA, October 10, 1987

As in case 1, a scan line as shown in Figure 10 was selected and model calculations were carried out for all 12 profile combinations for the NAA-SU path. The scan line is perpendicular to the NAA-SU path, ranges from −200 to 200 km, and is centered at the point of intersection of the NAA-SU and 485-SA paths. When results from the scans were found to be consistent with the data on the NAA-SU path, comparison was also made (using the same scan line) with the 485-SA path. The profile combination appearing most likely to have occurred based on agreement of polarity and magnitude of the amplitude changes between the data and modeling predictions on both paths was found to be 1B. Other model calculations were carried out to better match the data by varying the size of the disturbance.

Even with profile combination 1B, the 150-km-diameter disturbance size used resulted in VLF amplitude changes below the maximum values observed. Calculations with larger disturbance sizes indicate that a disturbance diameter of 300 km provides results consistent with the observed values. It is also possible, however, that the disturbance diameter was closer to ~150 km but that the flux levels were larger than 5×10^{-3} ergs cm^2 s^{-1} for the largest observed events. In the largest event observed, the NAA-SU perturbation was −0.5 dB, while that of 485-SA was 0.6 dB. When a surface plot was done for the NAA-SU case (shown in Figure 11 for the 400 × 400 km shaded region which is in Figure 10, using a 300-km disturbance and profile combination 1B), it was found that the largest perturbations were on the path and that the signal amplitude changes did not vary significantly with position along the path. However, the fact that the two crossing paths were simultaneously disturbed indicates that the disturbance is most likely to have occurred in the vicinity of the crossing point of the two paths.

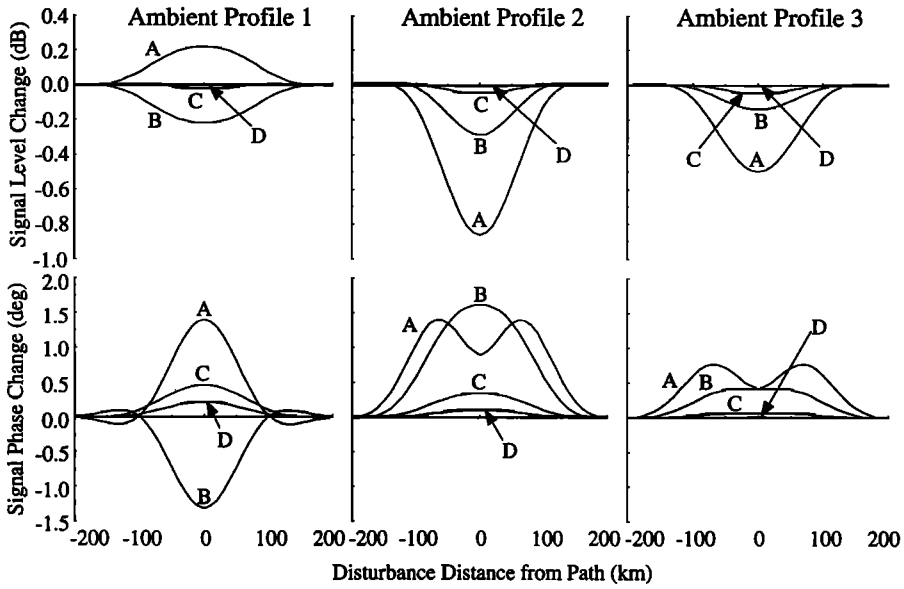

Figure 9. Each curve in the top row shows the predicted VLF signal amplitude change as a function of the location of a 150-km-diameter disturbance along the scan line shown in Figure 5. The curves are akin to that shown in Figure 6. The bottom row displays corresponding signal phase changes. Each column of the figure corresponds to one of the three ambient nighttime electron density profiles (Figure 3a). Curves are labeled to correspond to the electron density enhancements of Figure 3c.

Discussion

Case 1: NAU-LM, March 13, 1987

The lightning activity on this day was within ±150 km of the NAU-LM path [*Inan et al.*, 1988b]. It is quite possible that the lightning-disturbed ionospheric regions were at the same locations as the source; however, considering Figure 7, it is clear that disturbances anywhere along the path in the vicinity of the source lightning would have produced similar perturbations. Accordingly, we cannot determine the location of the disturbed ionospheric regions with respect to their position along the NAU-LM path. That the disturbed region in this case may not have been over the causative lightning discharges is consistent with other evidence indicating that magnetospheric conditions which favor whistler propagation and whistler-induced electron precipitation may well be more important than the location of the lightning in determining the location of the ionospheric disturbances [*Yip et al.*, 1991]. We recognize that the magnitude of a VLF perturbation signature of an LEP event depends on many factors such as lightning/whistler intensity, amounts of trapped and precipitated flux, the disturbance/duct spatial extent,

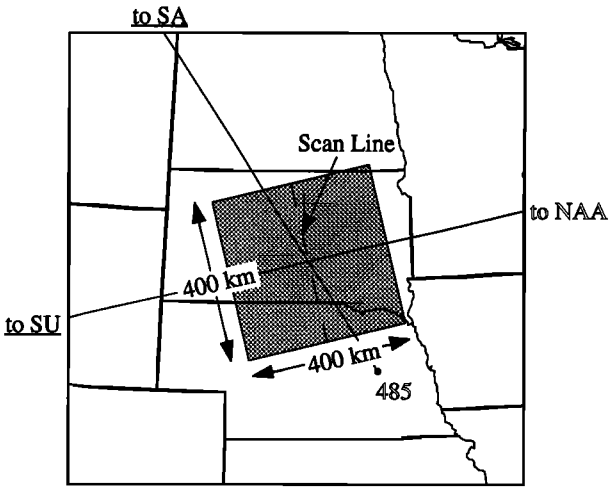

Figure 10. Map showing the region centered at the crossing point of the NAA-SU and 485-SA paths. The 400-km-long scan line indicates where the disturbance was located, as done in the NAU-LM case. The shaded square region is 400 × 400 km; it defines the disturbance locations used in generating Figure 11.

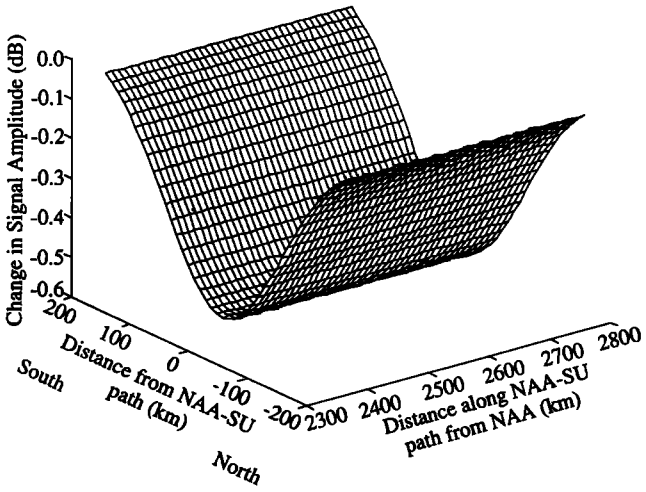

Figure 11. NAA signal amplitude change at SU due as a function of the disturbance's location, shown in a format similar to that of Figure 7. Profile combination 1B is used with a 300-km-diameter disturbance. The data is over the 400 × 400 km region shown in Figure 10. The lack of variation of signal amplitude with disturbance location parallel to the path is evident.

the energy spectra of the precipitated particles, the location of the disturbance with respect to the great circle path, and the ambient nighttime ionosphere. With this in mind, we are only able to give a likely upper bound on the spatial extent of the disturbance (250 km) and to locate it within about 100-200 km from the path, under the assumption of a reasonable value of flux (5×10^{-3} ergs cm^2 s^{-1}), when we employ a specific electron density ionospheric profile combination of ambient and enhanced density profiles.

Our major conclusion then, is that only one profile combination (2A) appears to be consistent with the amplitude of the VLF perturbations observed, if we assume a reasonable disturbed region size and flux level for the causative LEP events. This result implies that the nighttime *D* region conditions of ambient electron density profile 2 (Figure 3a) were likely in effect during this period and that the precipitation fluxes consisted of relatively high energy electrons as consistent with enhancement profile A. Enhancement profile A would be produced by precipitating electrons with energies > 600 keV, which at the *L* shell of the observation ($L \simeq 2.5$) would have been precipitated by whistler frequencies < 0.5 kHz [*Chang and Inan*, 1983]. There is no simultaneous whister data with which to assess this conclusion. However, data on radio atmospherics from the causative lightning flashes (which were measured at LM with the Stanford VLF broadband receiver) indicates strong excitation at frequencies < 1 kHz [*Inan et al.*, 1988b].

To gain further understanding of the effect of the ionospheric disturbance on the VLF signal, we examined the waveguide mode structure of the signals whose propagation we modeled. Figure 12 shows mode structure of the 28.5-kHz NAU signal in a polar plot format, showing both the relative amplitudes and phases of the vertical electric fields of the largest modes. Note that we are concerned only with the relative differences in amplitudes and phases of the modes in the direct and scattered signals. Since the phase changes are measured with respect to the phase of the direct (unperturbed) signal, no explicit phase reference is needed. The case shown is that which corresponds to a disturbance with diameter 150 km and located at the center of the scan line (Figure 5) for the electron density profile combination 2A. Figure 12a shows the modes which are excited at the transmitter. Figure 12b shows that only two dominant modes are present at the receiver under normal conditions. These two modes are the second and third quasi-transverse magnetic modes (QTM2 and QTM3) [*Poulsen et al.*, 1993]. In Figure 12c, we see the mode structure at the receiver of the signal scattered towards the receiver by the ionospheric disturbance. Once again, the QTM2 and QTM3 modes are dominant. The scattering results in a net change in the electrical path length for the modes with respect to the direct path, which accounts for the rotation of the mode vectors. Also, the relative magnitude of the QTM3 is somewhat higher in Figure 12c, indicating that this mode is more efficiently scattered than QTM2. Although weaker than the direct signal (Figure 12b), the vector addition of the scattered signal (Figure 12c) to the direct signal causes the observed change in signal amplitude.

Case 2: NAA-SU and 485-SA, October 10, 1987

The simultaneity of the LEP events observed on the two crossing VLF paths was the pointer to the geographic location of the events in case 2. As in case 1, one electron density profile combination stood out from the rest as providing results most consistent with the observed VLF amplitude perturbations. This profile combination was 1B, which corresponds to precipitating electrons with energies above 200 keV, and at the *L* shell of the observation ($L \simeq 3$) would be produced by whistler frequencies below 0.6 kHz [*Chang and Inan*, 1983].

Figure 13 shows polar plots for the dominant waveguide modes of the NAA-SU signal when a 300-km-diameter disturbance is located at the center of the scan line (Figure 10) with electron density profile combination 1B. As in Figure 12, the top panel (Figure 13a) shows the modes at the transmitter, the middle panel (Figure 13b) shows the modes at the receiver under ambient conditions, and the lower panel (Figure 13c) shows the mode structure of the scattered signal. The phase difference between the two signals arriving at the LM receiver (Figure 13b and 13c) in this case is also evident. The observed perturbation is produced by the vector addition of the ambient and scattered modes.

Summary

By comparing simulated effects of LEP-produced ionospheric disturbances on VLF signals with experimental data we were able

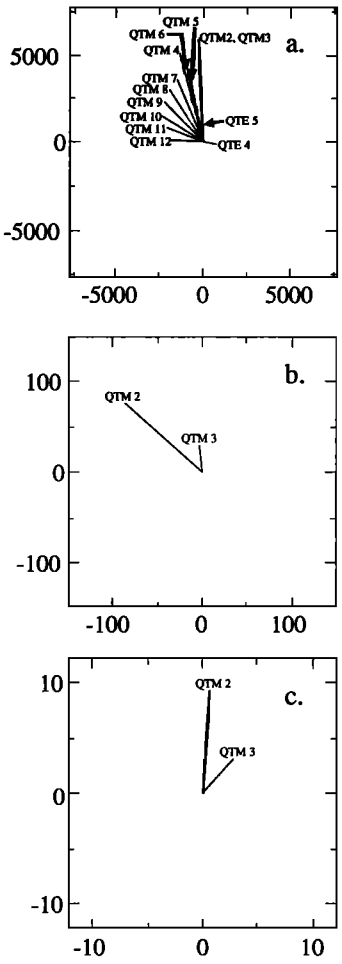

Figure 12. The waveguide mode structure of the NAU signal in polar plot format showing the relative amplitudes and phases of vertical electric fields corresponding to each mode. (a) The dominant modes excited at the transmitter. QTM (quasi-transverse magnetic) and QTE (quasi-transverse electric) modes are numbered by order. (b) The dominant modes arriving at the LM receiver under ambient conditions; so these modes propagate directly from the transmitter. (c) The mode structure at the receiver of the NAU signal scattered by the disturbance. The mode vectors are shown in arbitrary units since we are concerned only with changes in the signal (from LEP) and not actual signal levels. A disturbance 150 km in diameter and placed at the center of the scan line (Figure 5) was used with electron density profile combination 2A.

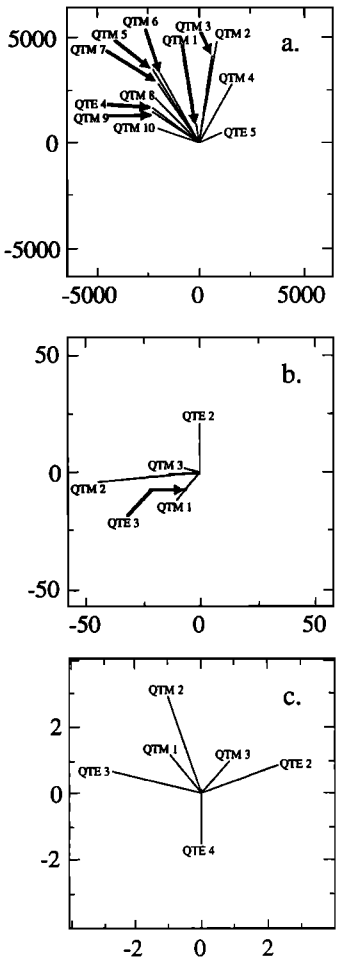

Figure 13. The waveguide mode structure of the NAA signal in polar plot format showing the relative amplitudes and phases of vertical electric fields corresponding to each mode. (a) The dominant modes excited at the transmitter. QTM (quasi-transverse magnetic) and QTE (quasi-transverse electric) modes are numbered by order. (b) The dominant modes arriving at the SU receiver under ambient conditions; so these modes propagate directly from the transmitter. (c) The mode structure at the receiver of the NAA signal scattered by the disturbance. The mode vectors are shown in arbitrary units since we are concerned only with changes in the signal (from LEP) and not actual signal levels. A disturbance 300 km in diameter and placed at the center of the scan line (Figure 10) was used with electron density profile combination 1B.

to assess the ionospheric electron density profiles most likely to have been in effect during the observed events. In two different cases we showed that one (but not the same one) electron density profile combination (the combination of specific ambient and disturbed profiles) provided results most consistent with data. The determination of the likely ionization enhancement profiles also represents a crude assesment of the energy spectrum of the precipitated flux in view of the correspondence between the precipitation energy spectra and the profiles A, B, C, D as indicated in Figure 4. At a fixed L shell, this information can in turn be used as an indicator of the upper frequency limit of the part of the ducted whistler spectrum which may have caused the precipitation of the energetic electrons (Figure 4).

It should be noted that our conclusions are based on waveguide propagation model calculations invoving a number of assumptions, as cited in section 3. Ionospheric or ground conductivity significantly different from those assumed may alter the modes of the signals and thus may affect the details of our conlusions. Nevertheless, the overall dependence of scattering on the location of the disturbance and on the ionospheric profile are not expected to be significantly different. As more cases with multiple disturbed adjacent and/or crossing VLF paths are analyzed, other characteristics of disturbances such as spatial extent and precipitated flux levels can be further understood in addition to the assessment of ionospheric electron density profiles.

Acknowledgments. We thank Martin Walt for his comments on the manuscript and to our colleagues in the STAR Laboratory for useful discussions. This research was sponsored by the National Science Foundation under grant ATM-9113012.

The Editor thanks J. C. Foster and A. R. Jacobson for their assistance in evaluating this paper.

References

Brace, L. H., and R. F. Theis, The behavior of the plasmapause at midlatitudes: ISIS-1 Langmuir probe measurements, *J. Geophys. Res.*, *79*, 1871, 1974.

Burgess, W. C., and U. S. Inan, The role of ducted whistlers in the precipitation loss and equilibrium flux of radiation belt electrons, *J. Geophys. Res.*, *98*, 15643, 1993.

Carpenter, D. L., and J. W. LaBelle, A study of whistlers correlated with bursts of electron precipitation near L=2, *J. Geophys. Res.*, *87*, 4427, 1982.

Chang, H. C., and U. S. Inan, Quasi-relativistic electron precipitation due to interactions with coherent VLF waves in the magnetosphere, *J. Geophys. Res.*, *88*, 318, 1983.

Chang, H. C., and U. S. Inan, Test particle modeling of wave-induced energetic electron precipitation, *J. Geophys. Res.*, *90*, 6409, 1985.

Helliwell, R. A., J. P. Katsufrakis, and M. L. Trimpi, Whistler-induced amplitude perturbation in VLF propagation, *J. Geophys. Res.*, *78*, 4679, 1973.

Inan, U. S., and D. L. Carpenter, On the correlation of whistlers and associated subionospheric VLF/LF perturbations, *J. Geophys. Res.*, *91*, 3106, 1986.

Inan, U. S., and D. L. Carpenter, Lightning-induced electron precipitation events observed at $L \sim 2.4$ as phase and amplitude perturbations on subionospheric VLF signals, *J. Geophys. Res.*, *92*, 3293, 1987.

Inan, U. S., W. C. Burgess, T. G. Wolf, D. C. Shafer, and R. E. Orville, Lightning-associated precipitation of MeV electrons from the inner radiation belt, *Geophys. Res. Lett.*, *15*, 172, 1988a.

Inan, U. S., D. C. Shafer, and W.-Y. Yip, Subionospheric VLF signatures of nighttime *D* region perturbation in the vicinity of lightning discharges, *J. Geophys. Res.*, *93*, 11455, 1988b.

Inan, U. S., M. Walt, H. D. Voss, and W. L. Imhof, Energy spectra and pitch angle distributions of lightning-induced electron precipitation: Analysis of an event observed on the S81-1 (SEEP) satellite, *J. Geophys. Res.*, *94*, 1379, 1989.

Inan, U. S., F. A.Knifsend, and J. Oh, Subionospheric VLF 'imaging' of lightning-induced electron precipitation from the magnetosphere, *J. Geophys. Res.*, *95*, 17217, 1990.

Inan, U. S., J. V. Rodriguez, S. Lev-Tov, and J. Oh, Ionospheric modification with a VLF transmitter, *Geophys. Res. Lett.*, *18*, 705, 1992.

Lohrey, B., and A. B. Kaiser, Whistler-induced anomolies in VLF propagation, *J. Geophys. Res.*, *84*, 5121, 1979.

Lyons, L. R., and R. M. Thorne, Equilibrium structure of radiation belt electrons, *J. Geophys. Res.*, *78*, 2142, 1973.

Park, C. G., D. L. Carpenter, and D. B. Wiggin, Electron density in the plasmasphere: whistler data on solar cycle, annual, and diurnal variations, *J. Geophys. Res.*, *83*, 3137, 1978.

Pasko, V. P., and U. S. Inan, Recovery signatures of lightning-associated VLF perturbations as a measure of the lower ionosphere, *J. Geophys. Res.*, *99*, 17523, 1994.

Poulsen, W. L., U. S. Inan, and T. F. Bell, A multiple-mode three-dimensional model of VLF propagation in the Earth-ionosphere waveguide in the presence of localized *D* region disturbances, *J. Geophys. Res.*, *98*, 1705, 1993.

Rawer, K., D. Bilitza, and S. Ramakrishnan, Goals and status of the International Reference Ionosphere, *Rev. Geophys.*, *16*, 177, 1978.

Reagan, J. B., R. E. Meyerott, R. C. Gunton, W. L. Imhof, E. E. Gaines, and T. R. Larsen, Modeling of the ambient and disturbed ionospheric media pertinent to ELF/VLF propagation, paper presented at NATO-AGARD Meeting on Medium, Long, and Very Long Wave Propagation, Brussels, Belgium, Sept. 1981.

Voss, H. D., W. L. Imhof, M. Walt, J. Mobilia, E. E. Gaines, J. B. Reagan, U. S. Inan, R. A. Helliwell, D. L. Carpenter, J. P. Katsufrakis, and H. C. Chang, Lightning-induced electron precipitation, *Nature*, *312*, 740, 1984.

Wait, J. R., and K. P. Spies, Characteristics of the Earth-ionosphere waveguide for VLF radio waves, *Tech. Note 300*, Nat. Bur. of Stand., Washington, D. C., 1964.

Yip, W.-Y., U. S. Inan, and R. E. Orville, On the spatial relationship between lightning discharges and propagation paths of perturbed subionospheric VLF/LF signals, *J. Geophys. Res.*, *96*, 249, 1991.

T. F. Bell, U. S. Inan, and S. J. Lev-Tov, STAR Laboratory, Department of Electrical Engineering, Durand 324, Stanford University, Stanford, CA 94305.

(Received February 21, 1995; revised May 25, 1995;
accepted May 25, 1995.)